Acta Pharmaceutica Sinica B 2021;11(10):3193−3205

Chinese Pharmaceutical Association
Institute of Materia Medica, Chinese Academy of Medical Sciences

Acta Pharmaceutica Sinica B

www.elsevier.com/locate/apsb
www.sciencedirect.com

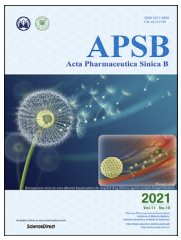

ORIGINAL ARTICLE

Ligand-based substituent-anchoring design of selective receptor-interacting protein kinase 1 necroptosis inhibitors for ulcerative colitis therapy

Jing Zhu[a,b,†], Meng Xin[a,c,†], Congcong Xu[a], Yuan He[d], Wannian Zhang[a,b], Zhibin Wang[a,*], Chunlin Zhuang[a,b,*]

[a]*School of Pharmacy, Second Military Medical University, Shanghai 200433, China*
[b]*School of Pharmacy, Ningxia Medical University, Yinchuan 750004, China*
[c]*Department of Pharmacy, Shanghai Municipal Hospital of Traditional Chinese Medicine, Shanghai 200071, China*
[d]*Tongji University Cancer Center, Shanghai Tenth People's Hospital, School of Medicine, Tongji University, Shanghai 200092, China*

Received 25 February 2021; received in revised form 29 April 2021; accepted 11 May 2021

KEY WORDS

Necroptosis;
RIP1;
RIP3;
Selectivity;
Ulcerative colitis

Abstract Receptor-interacting protein (RIP) kinase 1 is involved in immune-mediated inflammatory diseases including ulcerative colitis (UC) by regulating necroptosis and inflammation. Our group previously identified TAK-632 (**5**) as an effective necroptosis inhibitor by dual-targeting RIP1 and RIP3. In this study, using ligand-based substituent-anchoring design strategy, we focused on the benzothiazole ring to obtain a series of TAK-632 analogues showing significantly improving on the anti-necroptosis activity and RIP1 selectivity over RIP3. Among them, a conformational constrained fluorine-substituted derivative (**25**) exhibited 333-fold selectivity for RIP1 (K_d = 15 nmol/L) than RIP3 (K_d > 5000 nmol/L). This compound showed highly potent activity against cell necroptosis (EC_{50} = 8 nmol/L) and systemic inflammatory response syndrome (SIRS) induced by TNF-α *in vivo*. Especially, it was able to exhibit remarkable anti-inflammatory treatment efficacy in a DSS-induced mouse model of UC. Taken together, the highly potent, selective, orally active anti-necroptosis inhibitor represents promising candidate for clinical treatment of UC.

*Corresponding authors. Tel./fax: +86 21 81871204.
E-mail addresses: methyl@smmu.edu.cn (Zhibin Wang), zclnathan@163.com (Chunlin Zhuang).
†These authors made equal contributions to this work.
Peer review under responsibility of Chinese Pharmaceutical Association and Institute of Materia Medica, Chinese Academy of Medical Sciences.

https://doi.org/10.1016/j.apsb.2021.05.017

1. Introduction

Intestinal barrier integrity is one of the hallmarks of health, which is tightly linked to multiple human pathologies, including ulcerative colitis (UC)[1]. UC, a chronic inflammatory disease, is most commonly afflicting adults aged 30−40 years with a gradually increasing morbidity worldwide[2]. It is largely affecting human's daily life and has been classified as a modern refractory disease by World Health Organization. Severe diarrhoea, rectal bleeding and frequent abdominal pain are the common clinical symptoms of the UC patients along with persistent inflammation and ulcers in the intestinal mucosa[3]. Intestinal epithelium necroptosis is sufficient to induce and/or amplify inflammation, which may contribute to intestinal barrier dysfunction resulting in UC[4−7]. Recent evidence has supported that active receptor-interacting protein (RIP) kinase 1 can actuate inflammation through directly regulating necroptosis that is a caspase-independent, programmed necrosis[7,8]. RIP1 has represented as a master regulator of tumor necrosis factor α (TNF-α) mediated inflammatory pathology[9,10]. In addition to mediate detrimental responses downstream of TNF receptor 1 (TNFR1), RIP1 is also a key notion of inflammation downstream of toll-like receptors 3/4 (TLR3/4), Fas ligand (FasL), and TNF-related apoptosis-inducing ligand (TRAIL)[7,11−14]. The activated RIP1 enables the RIP1/RIP3/mixed lineage kinase domain-like protein (MLKL) pathway, and phosphorylated MLKL oligomerizes to trigger membrane rupture initiating necroptosis[15]. The necroptosis causes leakage of damage-associated molecular patterns (DAMPs), contributing to an intense inflammatory response[16]. Besides, RIP1 itself can also mediate the expression of inflammatory genes independently from necroptosis[17]. Thus, blocking RIP1 activation represents an opportunity and potentially benefits for the clinical treatment of necroptosis-related chronic inflammatory diseases, such as UC[7,9,15].

Yuan's group[18,19] pioneeringly identified a series of small-molecule inhibitors of RIP1, among which necrostatin-1s (Nec-1s, **1**, Fig. 1) was the most advanced compound showing excellent RIP1 selectivity. Currently, this compound has been investigated as a tool small molecule to evaluate the role of RIP1 and human diseases in animal models[16,20]. However, the subsequent development of this series of inhibitors has been limited, owing to a moderate potency, poor pharmacokinetic (PK) characteristics, and narrow structure−activity relationship (SAR) profile[21]. On the basis of a prioritized DNA-encoded library (DEL), GlaxoSmithKline (GSK) identified benzo[*b*][1,4]-oxazepin-4-ones as novel RIP1 inhibitor chemotypes[22,23]. A candidate GSK2982772 (**2**) has entered phase II clinical trials in patients of UC, psoriasis and rheumatic arthritis. GSK3145095 (**3**) was then developed with improved metabolic stability and has been carried out phase I trial for pancreatic adenocarcinoma[24]. Subsequently, GSK reported another novel chemotype of dihydropyrazoles as RIP1 inhibitors including GSK′547 (**4**)[25,26]. Denali Therapeutics developed a series of blood–brain barrier-penetrant RIP1 inhibitors with the chemical structure undisclosed, among which DNL104 was terminated due to limited post-dosing liver toxicity[9]. DNL747 is still in phase I clinical trials in patients with central degenerative diseases. It was reported that Lilly and Rigel Pharmaceuticals will jointly carry out the phase II clinical trial of R552 (undisclosed structure) in 2021[9,27].

In 2018, we identified TAK-632 (**5**, Fig. 2) from our fluorinated-compound library that effectively blocking necroptosis (HT-29, EC_{50} = 1.44 μmol/L) by dual-targeting RIP1 (K_d = 0.48 μmol/L) and RIP3 (K_d = 0.11 μmol/L), respectively[28]. Further optimizations by removing the cyano group on benzothiazole ring obtained compound **6** (SZM-594), which exhibited ∼8-fold improved anti-necroptotic activity (HT-29, EC_{50} = 0.17 μmol/L) and higher dual-targeting activity toward RIP1 (K_d = 0.1 μmol/L) and RIP3 (K_d = 0.08 μmol/L) kinases[28]. In addition, the carbamide replacement of the amide in the terminal trifluoromethylbenzyl group resulted in compound **7** (SZM-630) with good anti-necroptotic activity (HT-29, EC_{50} = 0.44 μmol/L) and high selectivity for RIP3 (K_d = 0.08 μmol/L) over RIP1 (K_d > 5 μmol/L)[29]. These results suggested that the benzyl part of TAK-632 might be the critical fragment for the selectivity of RIP3 over RIP1.

In this study, we focused on optimizations of the benzothiazole scaffold by a ligand-based substituent-anchoring design, aiming to improve the selectivity for RIP1 over RIP3. With this purpose, a fluorine-substituted benzothiazole derivative (**25**) was obtained showing > 333-fold selectivity for RIP1 than RIP3, and low nanomolar anti-necroptosis activity and *in vivo* efficacy toward UC were also observed.

2. Results and discussion

2.1. Design hypothesis

Our previous results have suggested that the benzyl part (R) of TAK-632 might be the critical fragment for the selectivity of RIP3 over RIP1[29]. We also predicted that the nitrogen of benzothiazole ring might form hydrogen-bonding interactions with the RIP1 and RIP3 kinases, however, the contribution to the kinase activity has not been confirmed yet[28,29]. On the other hand, the hydrogen-bonding interactions might be disrupted by changing the

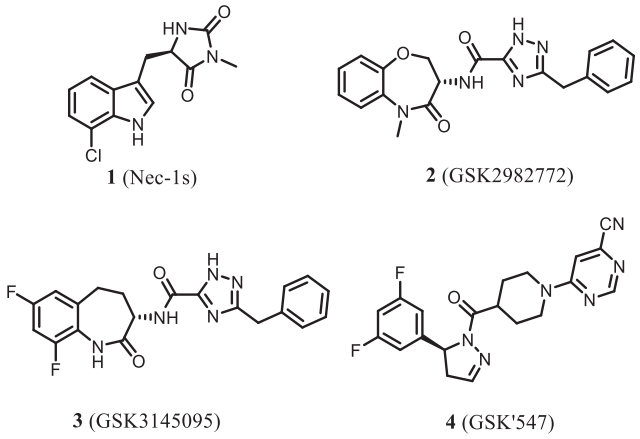

Figure 1 Representative RIP1 inhibitors.

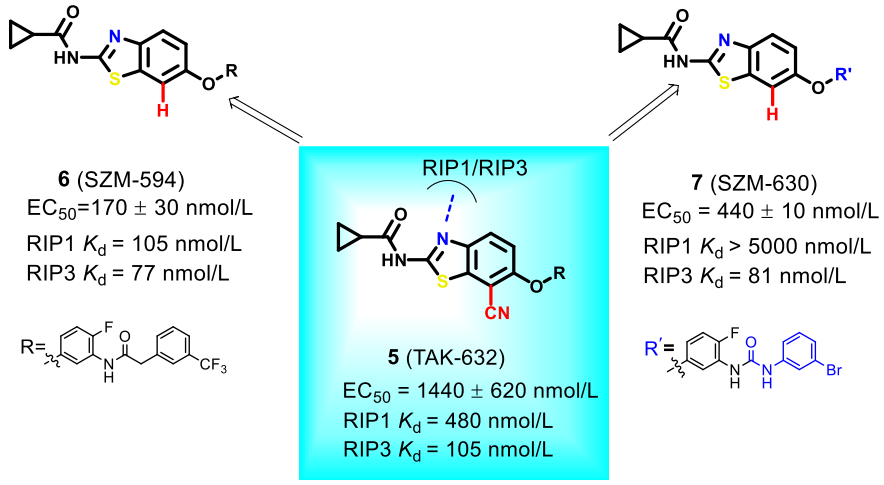

Figure 2 Our previous optimizations of TAK-632[28,29].

conformation of the benzothiazole ring, probably leading to different activity toward RIP1 and RIP3. TAK-632 with the C-7-substituent was suitable to both RIP1 and RIP3 with K_d values of 480 and 105 nmol/L. And the non-substituent on the benzene ring made compound SZM-594 flexible to interact with RIP1 and RIP3 (Fig. 3A), exhibiting higher activity than TAK-632 (C-7-CN). As illustrated in Fig. 3, when introducing substitutions on the different positions of the benzene ring, different benzothiazole conformations were generated. The C-4-substituted compounds bringing higher steric hindrance to the nitrogen side might have influence on the binding activity and selectivity toward RIP1/3 (Fig. 3B). The C-5-substituted compounds made the benzothiazole totally flipped (Fig. 3C), assuming that the flipped benzothiazole have great impact on the RIP1/3 selectivity. With these hypotheses, different substituents will be introduced to the benzothiazole ring in order to anchor the conformations of the scaffold to investigate the selectivity for RIP1 over RIP3.

2.2. *Chemistry*

To evaluate these three positions (C-4, C-5 and C-7) of the benzothiazole ring, structural variations on TAK-632 were performed and synthesized following previous publications[29,30]. As illustrated in Scheme 1, **m1** and 3-amino-4-fluorophenol were dissolved in dimethyl sulfoxide (DMSO), then K_2CO_3 was added to give the phenoxylated compounds **m2** in 60%−90% yields. Condensation of anilines **m2** with the 2-(3-(trifluoromethyl) phenyl)acetic acid HATU in dry pyridine obtained the acetamide derivatives **m3** in 50%−90% yields. Reducing the nitro group of **m3** got **m4** in 50%−80% yields. The intermediates **m4** reacting with bromine and KSCN successfully obtained the compounds **m5** in 50%−85% yields. The required compounds **10**−**11** were obtained by acylation of **m5** with cyclopropane carbonyl in dry pyridine at yields of 45%−90%. The carbonyl group of compound **10** was reduced using $NaBH_4$ in CH_3OH to obtain the

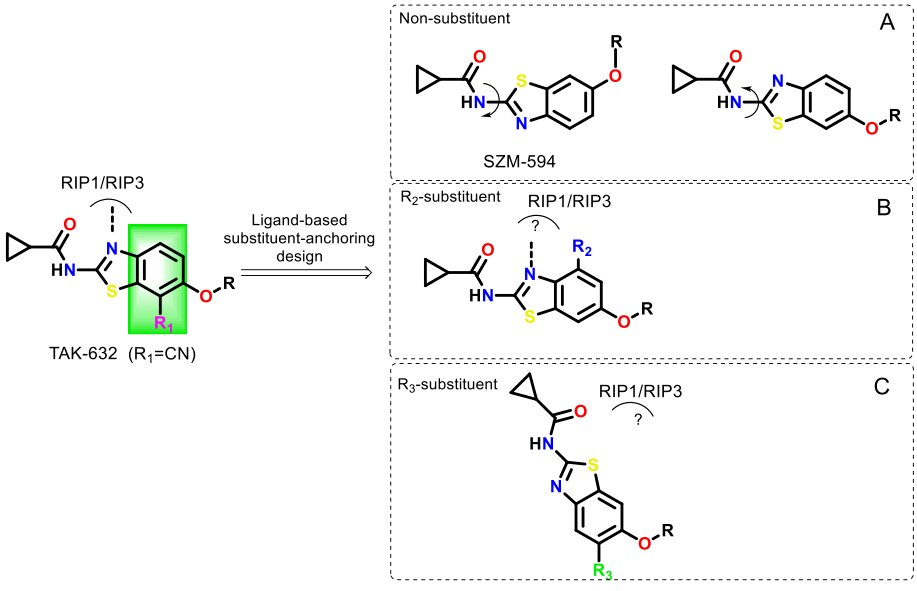

Figure 3 Design strategy of the benzothiazole scaffold.

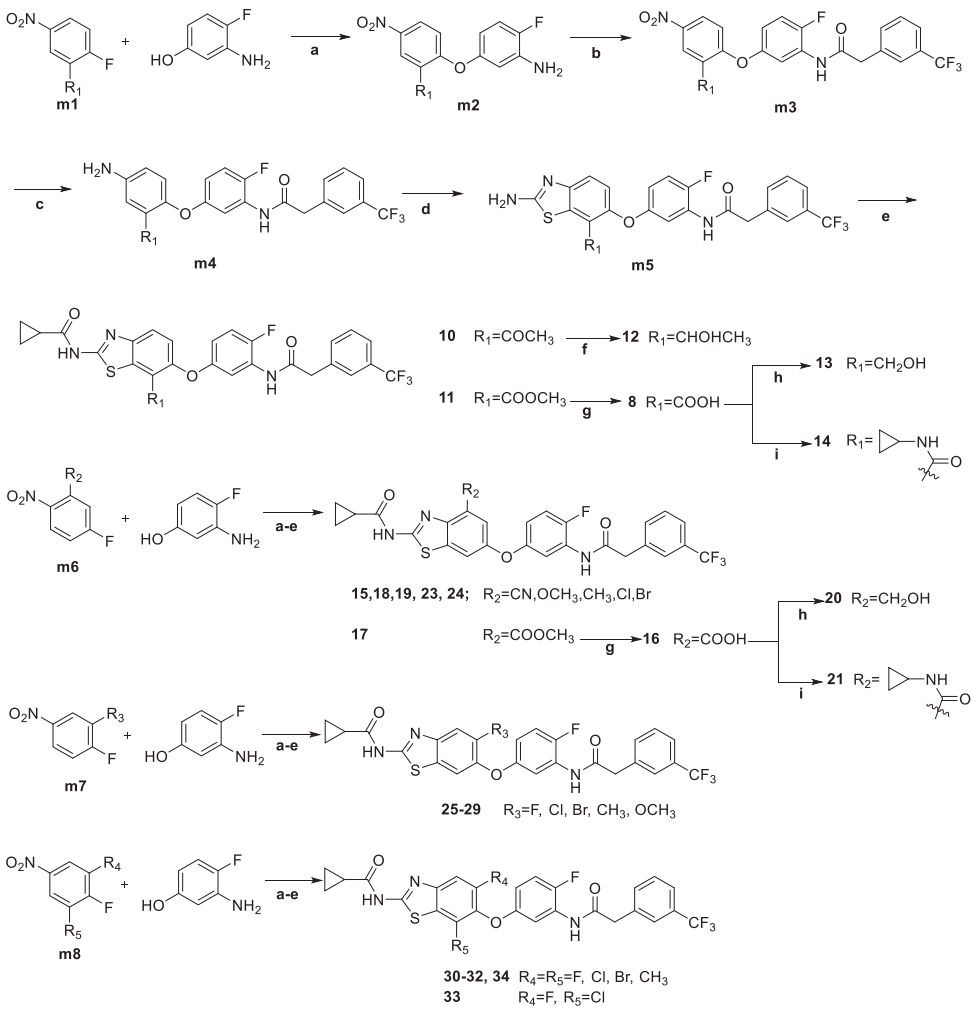

Scheme 1 Reagents and conditions: (a) K_2CO_3, DMSO, 90%–120 °C, 2 h, 40%–90%; (b) HATU, 2-(3-(trifluoromethyl)phenyl)acetic acid, Pyridine, 85 °C, N_2, 12 h, 50%–90%; (c) Fe, AcOH, 50 °C, 2 h, 50%–80%; (d) Br_2, KSCN, AcOH, r.t., 12 h, 20%–85%; (e) pyridine, N_2, 0 °C, r.t., 30%–90%; (f) $NaBH_4$, CH_3OH, 0 °C, 4 h, 60%; (g) CH_3OH, NaOH (4.5 mol/L), r.t., 1 h, 68%–80%; (h) THF, *iso*-butyl chloroformate, Et_3N, 0–4 °C, 0.6 h; then, THF, $NaBH_4$, CH_3OH, r.t., 3 h, 40%–51%; (i) DMF, HATU, DIPEA, cyclopropylamine, room temperature, 2 h, 31%–55%.

corresponding aniline **12** in a 60% yield. The methyl ester of compound **11** was hydrolyzed to the corresponding carboxylic acid using sodium hydroxide. The carboxyl group in **8** was reduced to obtain derivative **13** in two steps with a yield of 51%. Compound **14** was then obtained with cyclopropylamine using HATU as the coupling reagent. Compounds **15**, **17**–**19**, **23**–**24** with the mono-substitution R_2 on C-4 position were obtained following the same procedures (a–e) using **m6** as the starting material. Compounds **16**, **20** and **21** were obtained by the similar hydrolysis, reduction, and condensation reactions. Compounds **25**–**34** with the mono-substitution R_2 on C-5 position or di-substitutions (R_4, R_5) on C-5, C-7 positions were gave using the similar procedures with **m7** or **m8** as the starting material. For compound **9** with a C-7-NO_2 group, similar procedures (c, d, f–g in Scheme 2) with a different sequence were performed using 4-fluoro-3-nitroaniline as a starting material by reacting with **m9**. Compound **22** was synthesized through fluorination, reduction, condensation, cyclization, and acylation from a chlorinated intermediate **m11**.

The final structures were confirmed by ^{1}H NMR, ^{13}C NMR, and HRMS characterizations. In addition, the absolute configurations of compounds **25** (C-5-F) and **29** (C-5-OCH_3) were obtained by X-ray crystallography to confirm the regioselectivity of the 1,3-benzothiazole formation reaction. Compound **26** (C-5-Cl) was characterized by ^{1}H NMR, ^{13}C NMR, DEPT, HSQC, HMBC, ^{1}H–^{1}HCOSY and NOESY (Supporting Information).

2.3. *Structure optimizations and biological evaluation identify potent RIP1 inhibitors*

The ant-inecroptosis activity was measured using a chemiluminescence assay following our previous studies[28,29,31–33]. Different substitutions (R_1) at the C-7-position were introduced in the first round of optimizations (Table 1). Previously, the cyano group of TAK-632 was removed to obtain SZM-594 (**6**) showing much higher anti-necroptosis activity and target binding affinity, highlighting the substitutability of the cyano group[28]. When the cyano group was replaced by carboxyl group (**7**), no obvious anti-necroptosis activity was observed even at a high concentration of 10 μmol/L. The esterated analogue (**11**) exhibited a much better EC_{50} value of 23 ± 6 nmol/L. Then, the nitro group (**9**) was introduced, which showed a better activity (EC_{50} = 480 ± 10 nmol/L)

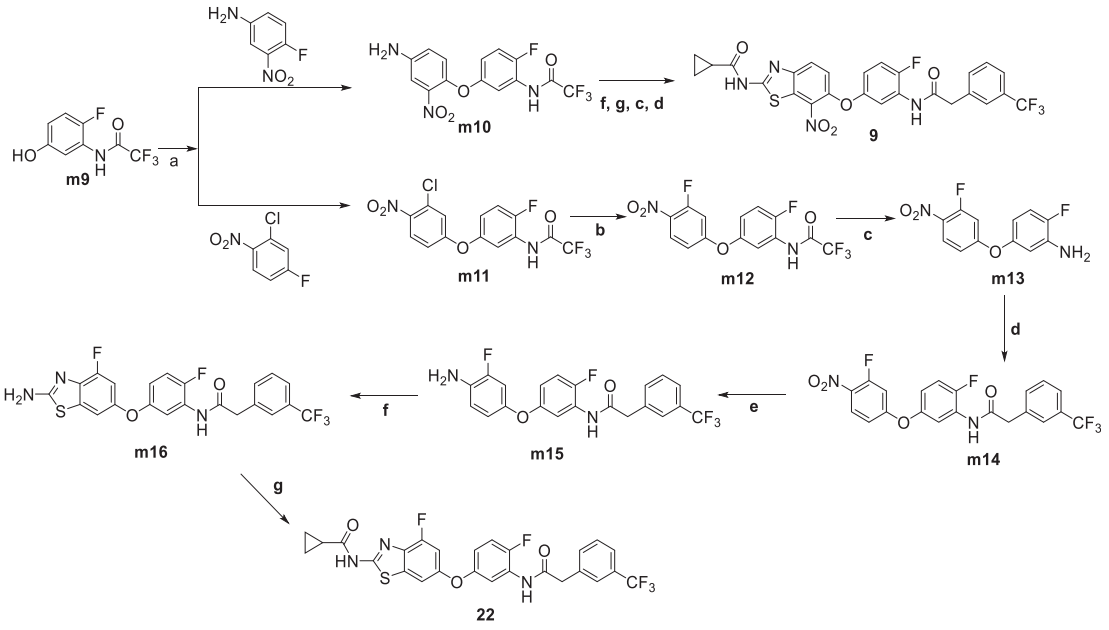

Scheme 2 Reagents and conditions: (a) K_2CO_3, DMSO, 90−120 °C, 2 h, 40%−90%; (b) CsF, DMSO, 120 °C, N_2, 12 h, 55%; (c) CH_3CH_2OH/CH_3OH (20:1), $NaBH_4$, 0 °C to r.t., 3 h, 63−91%; (d) HATU, 2-(3-(trifluoromethyl)phenyl)acetic acid, pyridine, 85 °C, N_2, 12 h, 55%−98%; (e) Fe, AcOH, 50 °C, 2 h, 60%; (f) Br_2, KSCN, AcOH, r.t., 12 h, 50%−73%; (g) pyridine, 0 °C to r.t., 68%−90%.

Table 1 First round of optimizations of TAK-632: evaluation on R_1.

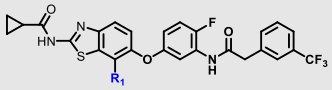

Compd.	R_1	Anti-necroptosis (EC_{50}, nmol/L)	Cytotoxicity (CC_{50}, μmol/L)	RIP1 (K_d, nmol/L)	RIP3 (K_d, nmol/L)	RIP1 selectivity
5 (TAK-632)[b]	CN	1440 ± 620	>50	480	105	0.22
6 (SZM-594)[b]	H	170 ± 30	36.5	97	77	0.79
8	COOH	>10,000	>50	N.D.[a]	N.D.	/
9	NO_2	480 ± 10	>50	710	260	0.37
10	$COCH_3$	130 ± 60	>50	880	330	0.37
11	$COOCH_3$	23 ± 6	>50	340	140	0.41
12	$CH(OH)CH_3$	45 ± 9	>50	22	140	6.4
13	CH_2OH	34 ± 1	>50	12	160	13
14		1036 ± 184	>50	N.D.	N.D.	/

[a]N.D. = not determined.
[b]These compounds have been included in our previous publications[28,29].

than TAK-632. A carbonyl group (**10**) greatly enhanced the activity in more than 10-fold (EC_{50} = 130 ± 60 nmol/L) than TAK-632. However, the RIP1 and RIP3 binding affinity of these compounds showed no significant change. When the carbonyl group of compound **10** was reduced, the obtained compound **12** exhibited a low nanomolar ranged activity (EC_{50} = 45 ± 9 nmol/L) and selectivity (6.4 fold) for RIP1 (K_d = 22 nmol/L) over RIP3 (K_d = 140 nmol/L). Compound **13** (R_1 = hydroxymethyl) showed acceptable activity (EC_{50} = 34 ± 1 nmol/L) and a high RIP1 binding affinity (K_d = 12 nmol/L) with 13-fold selectivity over RIP3 (K_d = 160 nmol/L). However, a cyclopropionyl group at the R_1 position (**14**) was unfavorable to the anti-necroptotic activity (EC_{50} = 1.036 μmol/L). Thus, these results indicated that the C-7-position of 1,3-benzothiazole was tolerated to some substituents and have influence on the RIP1 binding selectivity.

Then, we focused on C-4 position of the benzothiazole ring to evaluate the influence on the activity and kinase selectivity by different substitutions (R_2, Table 2). When the cyano group was removed to the R_2-position, compound **15** completely eliminated the activity. Besides, introducing carboxyl (**16**), ester (**17**), methoxy (**18**), methyl (**19**), hydroxymethyl (**20**), cyclopropionyl (**21**), chloro (**23**) and bromo (**24**) at this position showed no anti-necroptosis activities at 10 μmol/L. Even the small atom fluorine (**22**) made the activity dramatically decreased to an EC_{50} value of only 4.57 μmol/L compared with non-substituted SZM-594 (**6**), indicating the negative influence by the high steric hindrance on the nitrogen side. Considering the inactive anti-necroptosis property of these derivatives, the cytotoxicity and target binding affinity were meaninglessly evaluated.

Next, the substituents at the C-5-position (R_3, Table 3) were focused. With the synthetic condition of 1,3-benzothiazole

Table 2 Second round of optimizations of TAK-632: evaluation on R_2.

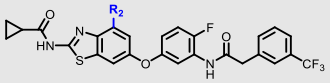

Compd.	R_2	Anti-necroptosis (EC_{50}, nmol/L)	Cytotoxicity (CC_{50}, μmol/L)	RIP1 (K_d, nmol/L)	RIP3 (K_d, nmol/L)	RIP1 selectivity
15	CN	>10,000	N.D.	N.D.	N.D.	/
16	COOH	>10,000	N.D.	N.D.	N.D.	/
17	$COOCH_3$	>10,000	N.D.	N.D.	N.D.	/
18	OCH_3	>10,000	N.D.	N.D.	N.D.	/
19	CH_3	>10,000	N.D.	N.D.	N.D.	/
20	CH_2OH	>10,000	N.D.	N.D.	N.D.	/
21		>10,000	N.D.	N.D.	N.D.	/
22	F	4570 ± 1220	N.D.	N.D.	N.D.	/
23	Cl	>10,000	N.D.	N.D.	N.D.	/
24	Br	>10,000	N.D.	N.D.	N.D.	/

Table 3 Third round of optimizations of TAK-632: Evaluation on R_3.

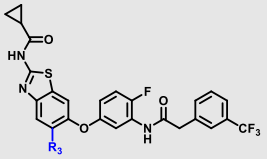

Compd.	R_3	Anti-necroptosis (EC_{50}, nmol/L)	Cytotoxicity (CC_{50}, μmol/L)	RIP1 (K_d, nmol/L)	RIP3 (K_d, nmol/L)	RIP1 selectivity
25	F	8 ± 1	>50	15	>5000	>333
26	Cl	44 ± 7	>50	36	>5000	>138
27	Br	170 ± 20	>50	180	>5000	>28
28	CH_3	60 ± 7	>50	140	>5000	>36
29	OCH_3	10 ± 2	>50	140	>5000	>36

formation reaction (Kaufmann's condition: KSCN, Br_2)[30], compounds with halogens (**25**–**27**), methyl (**28**) and methoxyl (**29**) were easier to obtain due to the regioselectivity. Compound **25** with C-5-F resulted in the best anti-necroptosis potency (EC_{50} = 8 ± 3 nmol/L) in this series, which was 180-fold higher than TAK-632 and 21-fold higher than SZM-594. Different from the previous derivatives, compound **25** showed significant RIP1 binding selectivity (>333-fold) with a K_d value of 15 nmol/L,

Table 4 Fourth round of optimizations of TAK-632: evaluation on di-substitutions.

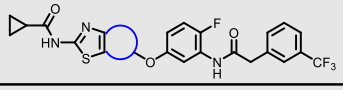

Compd.		Anti-necroptosis (EC_{50}, nmol/L)	Cytotoxicity (CC_{50}, μmol/L)	RIP1 (K_d, nmol/L)	RIP3 (K_d, nmol/L)	RIP1 selectivity
30		9 ± 2	>50	96	>5000	>52
31		180 ± 40	>50	64	>5000	>78
32		380 ± 10	>50	270	>5000	>19
33		76 ± 5	>50	37	>5000	>135
34		145 ± 10	>50	50	>5000	>100

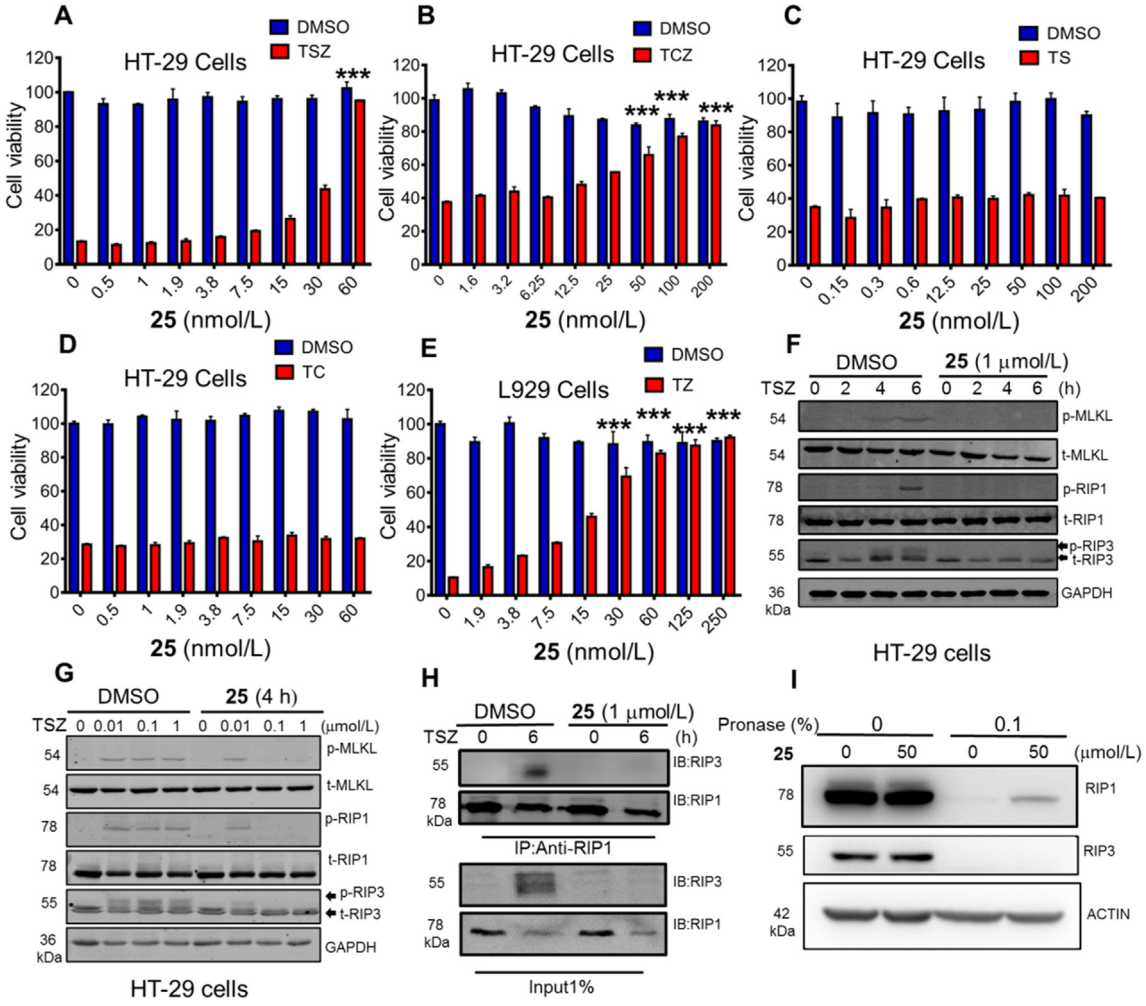

Figure 4 Anti-necroptosis effects of compound **25** *in vitro*. HT-29 cells were pretreated by compound **25** followed by incubation with TSZ (A), TCZ (B), TS (C) and TC (D) for 12, 24, 36 and 24 h, respectively. (E) L929 cells were pretreated with compound **25** followed by incubation with TZ for 9 h (***$P < 0.001$ *versus* stimulators without compound **25**). (F) HT-29 cells were pretreated with compound (1 μmol/L) followed by stimulation with TSZ at the indicated time points. Cells were lysed and immunoblotted with the indicated antibodies. (G) HT-29 cells were pretreated with compound (0, 0.01, 0.1, 1 μmol/L) and then stimulated with TSZ for 4 h. Cells were lysed and immunoblotted with the indicated antibodies. (H) HT-29 cells were treated with DMSO or compound **25** (1 μmol/L) for 6 h. The cell lysates were immunoprecipitated with anti-RIP1 antibody (IP: RIP1) and analyzed by Western blotting with an anti-RIP3 antibody (IB: RIP3). (I) DARTS analysis for **25**. HT-29 cell lysates were incubated with or without **25** (50 μmol/L) for 1 h and then digested with 0.1% Pronase for 30 min. Cells were lysed and immunoblotted with the indicated antibodies.

while no apparent activity was detected toward RIP3 even at 5000 nmol/L. The chloro- (**26**) and bromo- (**27**) substituted analogues possessed very similar biological results, showing high anti-necroptotic potencies and high selectivity for RIP1 over RIP3 (selectivity = 28−138). Moreover, the necroptosis inhibitory activities of the methyl- (**28**) and methoxyl- (**29**) analogues were 24–144-fold better compared with TAK-632. They also possessed good selectivity toward RIP1. In general, the RIP1 selectivity was decreased with the bulky enhancement of the substituents. These results confirmed our hypothesis that the flipped benzothiazole might anchor the conformations of the scaffold by the R_3 position for RIP1/3 selectivity, resulting in high anti-necroptotic potency.

In order to further confirm the importance of the C-5 position to the RIP1 selectivity, the di-substituted at C-5 and C-7 positions derivatives were generated (Table 4). Compound **30** with two fluorine atoms on the benzothiazole ring showed an RIP1/3 selectivity of >52 and its EC_{50} value was 9 ± 2 nmol/L. The di-chloro-substituted (**31**), di-bromo-substituted (**32**), and dimethyl-substituted (**34**) analogues exhibited good necroptosis inhibitory activities and more sensitive toward RIP1 than RIP3. Compound **33** with a fluorine and chlorine showed better selectivity (selectivity > 135) for RIP1 than **30** (difluoro-substituted, selectivity > 52) but lower anti-necroptosis activity. These results further suggested that the importance of C-5 position on the RIP1 selectivity.

2.4. *SAR analysis of the benzothiazole analogues*

With the above structural and biological information, SARs can be derived for further structural optimization: (1) The cyano group of TAK-632 was removable and replaceable. The C-7-position of the benzothiazole ring was tolerated for substituents and has influence on the RIP1 selectivity. (2) The C-4-position was intolerated to

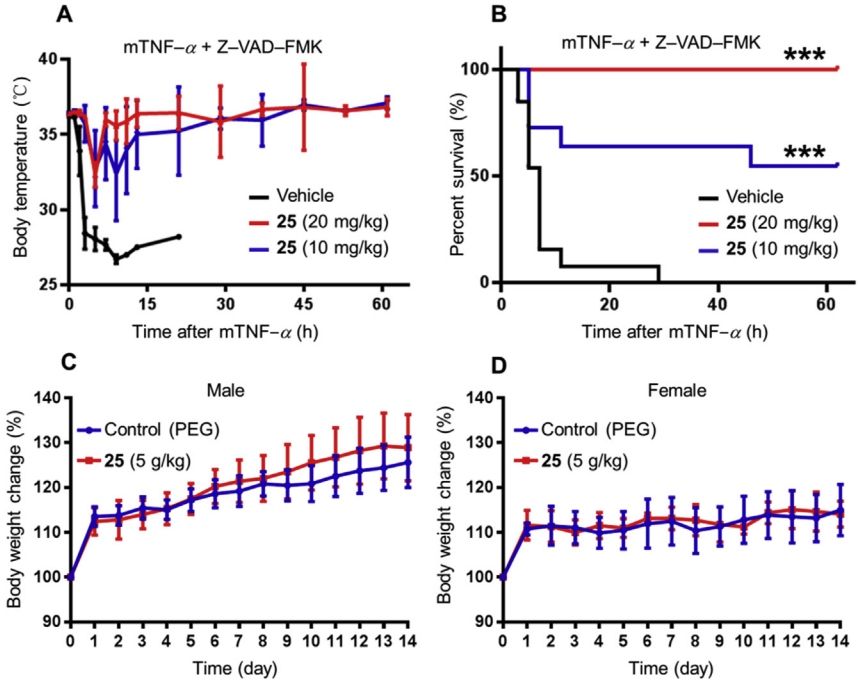

Figure 5 Anti-necroptosis and acute toxicity effects of compound **25** *in vivo*. (A) Body temperature of C57BL/6 mice ($n = 13-15$) injected with mTNF-α (150 μg/kg) after treatment with indicated doses of compound **25** (10 or 20 mg/kg) and (B) the survival curves (***$P < 0.001$ *versus* stimulators without compound **25**). (C) and (D) Acute toxicity of compound **25**. (C) Body weight change curves of male and (D) female mice during 14 days after a single oral administration of compound **25** (5 g/kg) or vehicle ($n = 10$).

any substituents. (3) The substituents at C-5-position by anchoring the conformation of the benzothiazole scaffold showed benefits on the anti-necroptosis activity, especially, the selectivity for RIP1 over RIP3. Furthermore, the derivatives with one more substituent at C-7-position confirmed the effect on RIP1 selectivity.

2.5. *Compound **25** inhibits necroptosis in vitro by selectively targeting RIP1*

Next, compound **25** was selected for the further biological evaluations due to the strongest anti-necroptotic activity in human HT-29 cells and the best RIP1 binding affinity and selectivity. Compound **25** could dose-dependently inhibit necroptosis induced by TSZ (Fig. 4A) or hTNF-α, cycloheximide, and Z-VAD-FMK (TCZ) (Fig. 4B). In the apoptosis model induced by hTNF-α plus cycloheximide (TC) or Smac mimetic (TS), compound **25** did not show any protective effects at different concentrations (Fig. 4C and D). We also confirmed that compound **25** dose-dependently attenuated necroptosis in murine L929 cells induced by mTNF-α and Z-VAD-FMK (TZ) (Fig. 4E). These results collectively indicated that compound **25** specifically inhibited the activation of necroptosis.

Then, we investigated the phosphorylation of RIP1, RIP3, and MLKL in TSZ-induced HT-29 cells pretreated with compound **25**, aiming to clarify the blocking effect of **25** on the necroptosis pathway. Considering the RIP1 is a upstream regulator of RIP3, the phosphorylation level of RIP3 is affected by both the kinase activity of RIP3 itself and RIP1[34]. As shown in Fig. 4F, the selective RIP1 inhibitor **25** could completely inhibit the phosphorylation of RIP1 and RIP3 at 1 μmol/L within 6 h. Subsequently, the downstream phosphorylation of MLKL was also completely inhibited. As shown in Fig. 4G, compound **25** inhibited the phosphorylation of RIP1/3 and MLKL at 4 h after TSZ induction in a dose−response manner (0, 0.01, 0.1 and 1 μmol/L). Then, we detected the RIP1-RIP3 necrosome formation in HT-29 cells, which requires the phosphorylation of RIP1 and RIP3[35]. After pretreated with compound **25**, it completely blocked TSZ-induced necrosome formation for inhibiting the necroptosis (Fig. 4H). Due to the strong RIP1 selectivity of compound **25**, we speculated whether **25** interacted with RIP1 directly. Here, we employed drug affinity responsive target stability assay (DARTS)[28], which relies on the reduction of protease susceptibility of the direct target protein upon drug binding, to detect the potential interaction between **25** and RIP1/3 kinases. As shown in Fig. 4I, RIP1 was protected from protease digestion in the extract of **25**-treated cells, whereas RIP3 was not detected in the same sample, indicating that **25** may interact with RIP1 but not RIP3, consistent with the biochemical assay.

2.6. *Compound **25** inhibits RIP1-dependent systemic inflammatory response syndrome (SIRS) and exhibits no apparent toxicity in vivo*

In vivo, the RIP1-dependent SIRS model characterized by hypothermia[36], was applied to explore the protective efficacy of compound **25**. Compound **25** (10 or 20 mg/kg, intragastric administration) protected mice from body temperature loss in the first 2−3 h after treatment with mTNF-α (intravenous injection)/Z-VAD-FMK (intragastric administration), which was dramatically different from the model mice (Fig. 5A). As shown in Fig. 5B, compound **25** dose-dependently improved the survival rate of the SIRS mice. Mice administrated with a single dose of **25** (10 or 20 mg/kg) exhibited survival rate of 60% and 100% in over 60 h, much higher than the TNF-α group (mice were totally died in about 30 h).

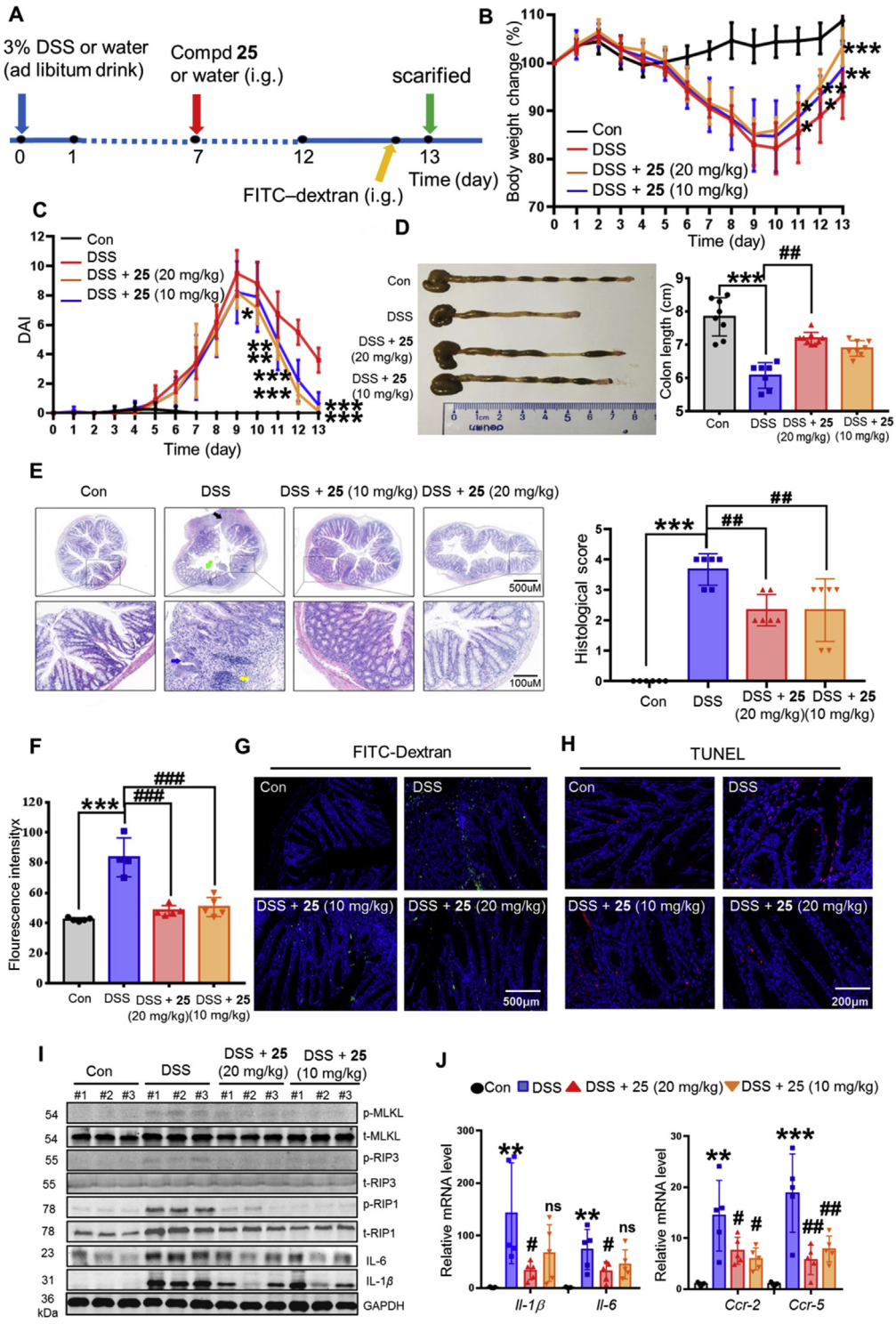

Figure 6 Compound **25** alleviates DSS-induced UC *in vivo*. (A) Experimental design of 3% DSS-induced UC model and treated with compound **25** ($n = 8-10$). Except the normal control group, mice in other groups were given DSS dissolved in sterile drinking water for 7 days to induce UC. From Day 7−13, mice in the control group, model group and administration group were given water, vehicle (0.5% sodium carboxymethyl cellulose) and compound **25** (10 or 20 mg/kg) by intragastric administration, respectively. After the mice were sacrificed, the colons and serum were collected on Day 13. (B) Body weight change curves during experiment. (C) DAI score change curves during experiment. (D) Length of the colons on Day 13. (E) Representative pictures of H&E-stained and histological scores of colons (Black arrow: ulceration; Green arrow: mucosal epithelial cells; Blue arrow: goblet cells; Yellow arrow: inflammatory cells infiltration). (F) The serum levels of FITC-dextran in each group of mice. (G) FITC-dextran in colon tissues of different groups. (H) Analysis of intestinal epithelial cell injuries by TUNEL. (I) Western blot analysis of the biomarkers of necroptosis and IL-1β and IL-6 in colonic tissues. GAPDH is used as the control for protein loading. (J) Quantitative analysis of inflammatory cytokines RNA extracted from colon tissues of mice. $^{*}P < 0.05$, $^{**}P < 0.01$, and $^{***}P < 0.001$ *versus* control-group, $^{\#}P < 0.05$, $^{\#\#}P < 0.01$, and $^{\#\#\#}P < 0.001$ *versus* DSS-model group.

Before we evaluated the efficacy of **25** in the UC model, a single-dose acute toxicity test of **25** was carried out in healthy mice at a dose of 5 g/kg (the extremely low toxicity) according to the criteria of "Chemicals-Test method of acute oral toxicity (GB/T21603-2008)". As a result, no death occurred after intragastric administration of **25** in 2 weeks. All mice in the drug administration groups (male and female) grew normally (the same as the mice in the control groups). The body weights of these mice gradually increased (Fig. 5C and D), and no significant behavioral abnormalities were observed over the 14-day period. Therefore, **25** was well tolerated at a dose of 5 g/kg with no acute toxicity. These results support the potential of **25** as a safe candidate for further investigations.

2.7. *Compound* **25** *alleviates dextran sulfate sodium (DSS)-induced UC in vivo*

The therapeutic efficacy of compound **25** was further evaluated in the DSS-induced UC model. Seven days after administration of DSS, the mice were intragastrically treated with another 6-day course of compound **25** to evaluate its therapeutic potency (Fig. 6A). As shown in Fig. 6B, the body weights of DSS-treated mice were seriously decreased in the first 9 days and slowly alleviated. Starting from Day 11, the 4th day of treatment, the alleviation of body weight of the mice treated with compound **25** was significantly dose-responsed speeded up. Disease activity index (DAI) is then applied to quantitatively analyze the weight loss, stool consistency, and stool blood of UC mice[37]. Compared with untreated UC mice, DAI of **25**-treated mice was decreased more quickly dose-dependently (Fig. 6C). Meanwhile, the mice treated with compound **25** at a dose of 20 mg/kg showed longer colon length ($P < 0.01$) than untreated colitis mice (Fig. 6D). The histopathological analysis revealed that compound **25** significantly alleviated the areas of ulceration, the loss of mucosal epithelium and goblet cells, and inflammatory cells infiltration (Fig. 6E). Furthermore, the protective effect of compound **25** on the intestinal barrier function was investigated in the fluorescein isothiocyanate (FITC)-dextran permeability assay of the intestinal epithelium. The level of FITC-dextran in the serum of treated mice was significantly lower than that of DSS-disease mice (Fig. 6F). The fluorescence imaging also showed reduced infiltration of FITC-dextran into the colon submucosa in the **25**-treated mice (Fig. 6G). TUNEL staining (Fig. 6H) and Western blot assays (Fig. 6I) indicated that compound **25** effectively inhibited necroptosis pathway by reducing the phosphorylation of RIP1, RIP3 and MLKL. Additionally, compound **25** inhibited the protein expressions of IL-6 and IL-1β in colon tissue in a dose−response manner (Fig. 6I). Moreover, compound **25** significantly reduced the mRNA of inflammatory cytokines (*Il-6* and *Il-1β*) and chemokine receptors (*Ccr-2* and *Ccr-5*) (Fig. 6J).

Table 5 PK profile of compound **25**.[a]

Parameter	1 mg/kg (i.v.)	10 mg/kg (*p.o.*)
$t_{1/2}$ (h)	1.67 ± 0.46	1.18 ± 0.62
T_{max} (h)	–	0.67 ± 0.29
C_{max} (ng/mL)	–	381 ± 35
AUC_{0-t} (h·ng/mL)	1030 ± 350	991 ± 218
$AUC_{0-\infty}$ (h·ng/mL)	1060 ± 354	1027 ± 245
CL (mL/min/kg)	16.8 ± 4.8	–
V_{SS} (L/kg)	1667 ± 856	–
MRT_{inf} (h)	1.59 ± 0.43	2.74 ± 0.32
F (%)	–	9.69 ± 2.31

[a]PK parameters (mean ± SD, $n = 9$).

2.8. *The pharmacokinetic properties of compound* **25** *in mice*

The pharmacokinetic (PK) characteristics of compound **25** in mice were also evaluated. The key *p.o.* and i.v. administration PK parameters are summarized in Table 5. After a single i.v. administration with 1 mg/kg compound **25**, the half time ($t_{1/2}$), the clearance rate (CL) and apparent distribution volume (V_{ss}) of **25** were 1.67 h, 16.8 mL/min/kg, and 1667 L/kg, respectively. When **25** was administrated by oral route at 10 mg/kg, its half time ($t_{1/2}$), maximum plasma concentration (C_{max}) and oral bioavailability (*F*) were 1.18 ± 0.62 h, 381 ± 35 ng/mL and 9.69 ± 2.31%, respectively.

3. Conclusions

With the purpose to improve the selectivity for RIP1 over RIP3 of the lead compound TAK-632, we focused on the benzothiazole ring by four rounds of structural optimizations *via* a ligand-based anchoring design strategy. The three (C-4, C-5 and C-7) positions were evaluated to obtain highly selective RIP1 inhibitors with very potent anti-necroptosis activity and low cytotoxicity. An obvious SAR of the benzothiazole ring was summarized to guide further optimizations. Of the newly synthesized analogues, compound **25** exhibited more than 333-fold selectivity for RIP1 over RIP3 and showed the best anti-necroptotic activity *in vitro* and *in vivo*. Especially, this compound possessed significant therapeutic efficacy in a DSS-induced UC model with apparent anti-inflammatory effects by reducing the phosphorylation of RIP1, RIP3 and MLKL in the colonic tissues. Thus, this C-5-F substituent-anchoring benzothiazole compound represents a promising candidate for future development of anti-UC drugs.

4. Experimental

4.1. *Chemistry*

The detailed chemistry procedures were presented in Supporting Information. The ^{1}H NMR, ^{13}C NMR, DEPT, HSQC, HMBC, ^{1}H−^{1}H COSY and NOESY spectra, X-ray crystal structures and HPLC chromatograms showing the purity of the target compounds (DOCX).

4.1.1. *N-(5-Fluoro-6-(4-fluoro-3-(2-(3-(trifluoromethyl)phenyl) acetamido)phenoxy)benzo[d]thiazol-2-yl) cyclopropanecarboxamide (***25***)*

White solid, Yield: 80%, mp 210−211 °C. ^{1}H NMR (300 MHz, DMSO-d_6) δ 12.74 (s, 1H, NH), 10.13 (s, 1H, NH), 7.86 (d, J = 8.1 Hz, 1H), 7.76 (d, J = 11.4 Hz, 1H), 7.66 (s, 2H), 7.63−7.51 (m, 3H), 7.27 (t, J = 9.9 Hz, 1H), 6.80−6.74 (m, 1H), 3.85 (s, 2H, CH_2), 2.01−1.95 (m, 1H), 0.97−0.95 (m, 4H). ^{13}C NMR (150 MHz, DMSO-d_6) δ 173.3, 169.7, 160.2, 153.8, 152.8, 148.6, 146.2, 140.0, 137.5, 134.0, 129.8, 129.4, 128.1, 127.6, 126.3, 123.9, 116.8, 116.6, 115.3, 113.1, 111.6, 108.7, 42.5, 14.3, 9.2. HRMS *m/z* $C_{26}H_{18}F_5N_3O_3S$: Calcd. 548.1068, found 548.1064 $[M+H]^+$.

4.2. Biology

4.2.1. Biology reagents

Recombinant mouse mTNF-α (CF09) and human hTNF-α (C008) were obtained from Novoprotein. PMSF, phosphatase inhibitor mixture and protease inhibitor cocktail (WB0122) were obtained from Shanghai Weiao Biotechnology.

4.2.2. Commercial antibodies

Anti-human antibodies: RIP1 (3493s) and phospho-RIP1 (65746s) were obtained from Cell Signaling Technology. RIP3 (ab209384), phospho-RIP3 (ab209384), MLKL (ab184718), phospho-MLKL (ab187091) and GAPDH (ab181602) were obtained from Abcam.

Anti-mouse antibodies: phospho-RIP1 (38662) from Cell Signaling Technology, RIP3 (17563-1-AP), IL-6 (66146-1-lg), IL-1β (26048-4-AP) and MLKL (66675-1-Ig) were obtained from Proteintech, phospho-RIP3 (ab195117) and phospho-MLKL (ab196436) were obtained from Abcam.

4.2.3. Cell culture

HT-29 (NCI-DTP Cat# HT-29) and L929 (ECACC Cat# 14112101) cells were purchased and cultured in DMEM containing 10% FBS, 100 U/mL streptomycin/penicillin and 1% L-glutamine in humidified atmosphere of 5% CO_2 at 37 °C.

4.2.4. Anti-necroptosis activity assays

Necroptosis of HT-29 cells was caused by pretreatment with Smac mimetic (10 nmol/L) and Z-VAD-FMK (20 μmol/L) or TCZ for 0.5 h followed by incubation with hTNF-α (20 ng/mL) for the specified time. Apoptosis was induced by incubation with TS or TC for the specified time. The cell viability was measured using the CellTiter-Glo Luminescent Cell Viability Assay kit (Beyotime, C0065L). The luminescences were recorded with Molecular Devices (SpectraMax M5). All experiments were triplicated performed independently.

4.2.5. Kinase assay

The inhibitory effects on RIP1 and RIP3 kinases were detected by a KINOMEscan™ assay. The experiments were duplicated conducted, and the K_d values are presented as the average.

4.2.6. Immunoblotting

After compound **25** intervention, the cells or colon tissues were lysed using NP-40 buffer (Beyotime Biotechnology, P013F) containing protease/phosphatase inhibitors and PMSF. The samples (20 μg) were resolved over 10% SDS-PAGE and transferred to NC membranes. The membranes were then blocked in 5% NOT-Fat Powdered milk (Sangon Biotech, A600669-0250), incubated with primary antibodies (1:1000) and secondary antibody (1:10000) that diluted in 5% milk. The blotting results were analyzed using the LI-COR Odyssey system.

4.2.7. Immunoprecipitation

After 6 h treatment of compound **25**, HT-29 cells were lysed and incubated with anti-RIP1 antibody and Protein A/G agarose successively at 4 °C for two days. The immunoprecipitated proteins were obtained by boiling in 2 × SDS buffer and examined by Western blot analysis.

4.2.8. Drug affinity responsive target stability assay

DARTS experiments for identifying the targets of **25** were performed as our previous reports[28,38]. Cells were lysed and treated with **25** (50 μmol/L) followed by digestion with 0.1% pronase for 30 min at room temperature. The digestion was stopped by directly adding SDS-PAGE loading buffer and Pronase inactivated by boiling. Protein samples were separated with 10% SDS-PAGE and analyzed by immunoblotting.

4.2.9. FITC-dextran intestinal permeability assay

FITC-dextran (Sigma, FD4, 600 mg/kg), a permeability probe, was given by gavage 4 h before the mice were killed. Then, the levels of FITC-dextran in serum were detected by fluorometry (Ex: 488 nm, Em: 525 nm) with Molecular Devices (SpectraMax M5).

4.2.10. H&E and TUNEL staining

The colon tissue of mice was fixed with 4% paraformaldehyde and embedded in paraffin. Each paraffin block was sectioned at 4 μm and stained with hematoxylin and eosin (H&E, Servicebio, G1005) and TUNEL (Servicebio, GB1502).

4.2.11. Quantitative real-time PCR

Total RNA was extracted from tissue homogenates of colon with RNAiso Plus reagent (TaKaRa, 9109). The cDNA was synthesized with a PrimeScript RT Master Mix kit (TaKaRa, RR036A). Quantitative RT-PCR was executed using PowerUp SYBR Green Master Mix (Thermo Fisher Scientific, A25742). Resulting cDNA was then used as a template for qPCR on the instrument (Roche, LightCyccler96). Primers for the inflammatory factors and internal reference were summarized in Supporting Information Table S1.

4.3. Animal experiments

4.3.1. SIRS

Animal experiments were approved by the Second Military Medical University Committee on Animal Care (Shanghai, China). Female C57BL/6 J mice (weight 18−22 g, n = 13−15) obtained from SIPPR-BK biochemistry Co. (Shanghai, China, SCXK2018-0006) were given compound **25** one hour before mTNF-α intravenously injection (150 μg/kg). After 15 min, Z-VAD-FMK (180 μg) was administrated by oral gavage. Another dose of Z-VAD-FMK (70 μg) was administrated 1 h after mTNF-α injection.

4.3.2. DSS-induced UC model

Female C57BL/6 J mice were divided into four groups: A) Control group (group 1); B) DSS (MP Biomedicals, 36,000−50,000 Da)-induced colitis group (group 2); C) DSS-induced colitis plus high dose (20 mg/kg) of **25**-treated group (group 3); and D) DSS-induced colitis with low dose (10 mg/kg) of **25**-treated group (group 4). Each group consisted of 8−10 mice. Mice in group 1 received drinking water alone and were used as negative controls. Colitis was induced in mice of groups 2−4 by administration of DSS (3%, *w*/*v*) for 7 days. Mice in groups 3 and 4 were given high and low doses of **25** *via* oral gavage once a day for six consecutive days after the DSS treatment period. At the 13th day, all animals were sacrificed by dislocation of the cervical vertebra for blood and colonic tissues collection.

4.3.3. PK study

Male ICR mice (18−22 g, Chengdu Dashuo Laboratory Animal Co. SCXK2015-030) were used in the PK studies. The compound was dissolved and vortexed in 5% DMSO, 5% HS-15, and 90%

physiological saline for a concentration of 0.1 mg/mL for intravenous injection group. The compound was dissolved and vortexed in 0.5% CMC-Na (including 1% DMSO) for a concentration of 1 mg/mL for intragastric administration group. The mice were housed in a room with controlled temperature and humidity and allowed free access to food and water. The male ICR mice were split into intravenous injection group (**25**, 1 mg/kg, $n = 9$) and intragastric administration group (**25**, 10 mg/kg, $n = 9$) before starting treatment. At different time points, the blood samples were collected and centrifuged at 4 °C to obtain plasma, which was stored at −80 °C until analysis by LC/MS/MS. PK parameters were determined from individual animal data using non-compartmental analysis in winNonlin 6.3.

4.3.4. Acute toxicity assay

Compound **25** was firstly suspended in PEG400 solution. Twenty male and twenty female mice (16−19 g, Beijing Vital River Laboratory Animal Technology Co., SCXK2017-0011) were randomly divided into four groups ($n = 10$/group): male control group, female control group, male test group, and female test group. After fasting for 12 h, mice in test groups were given **25** intragastrically at a dose of 5 g/kg, and the mice in control groups were given the same volume of vehicle solution. The death, abnormal behaviors and body weight of these mice were monitored every day during the subsequent two weeks.

Acknowledgments

This work was funded by grants from the National Natural Science Foundation of China (82022065, 81872791, 81872880, 82073696, and U20A20136); the Sanhang Program of Second Military Medical University, and the Key Research and Development Program of Ningxia (2019BFG02017, China).

Author contributions

Ideas and experiment design: Chunlin Zhuang and Zhibin Wang; Medicinal chemistry: Jing Zhu, Congcong Xu and Chunlin Zhuang; Biology: Meng Xin, Jing Zhu, Yuan He, and Zhibin Wang; Analysis and data interpretation: All; Writing and review of the manuscript: All; Study supervision and funding: Chunlin Zhuang, Zhibin Wang and Wannian Zhang.

Conflicts of interest

The authors have no conflicts of interest to declare.

Appendix A. Supporting information

Supporting information to this article can be found online at https://doi.org/10.1016/j.apsb.2021.05.017.

References

1. Lopez-Otin C, Kroemer G. Hallmarks of health. *Cell* 2021;**184**:33−63.
2. Ungaro R, Mehandru S, Allen PB, Peyrin-Biroulet L, Colombel JF. Ulcerative colitis. *Lancet* 2017;**389**:1756−70.
3. Kobayashi T, Siegmund B, Le Berre C, Wei SC, Ferrante M, Shen B, et al. Ulcerative colitis. *Nat Rev Dis Primers* 2020;**6**:74.
4. Vereecke L, Beyaert R, van Loo G. Enterocyte death and intestinal barrier maintenance in homeostasis and disease. *Trends Mol Med* 2011;**17**:584−93.
5. Gunther C, Neumann H, Neurath MF, Becker C. Apoptosis, necrosis and necroptosis: cell death regulation in the intestinal epithelium. *Gut* 2013;**62**:1062−71.
6. Pierdomenico M, Negroni A, Stronati L, Vitali R, Prete E, Bertin J, et al. Necroptosis is active in children with inflammatory bowel disease and contributes to heighten intestinal inflammation. *Am J Gastroenterol* 2014;**109**:279−87.
7. Pasparakis M, Vandenabeele P. Necroptosis and its role in inflammation. *Nature* 2015;**517**:311−20.
8. Silke J, Rickard JA, Gerlic M. The diverse role of RIP kinases in necroptosis and inflammation. *Nat Immunol* 2015;**16**:689−97.
9. Mifflin L, Ofengeim D, Yuan J. Receptor-interacting protein kinase 1 (RIPK1) as a therapeutic target. *Nat Rev Drug Discov* 2020;**19**:553−71.
10. Ofengeim D, Yuan J. Regulation of RIP1 kinase signalling at the crossroads of inflammation and cell death. *Nat Rev Mol Cell Biol* 2013;**14**:727−36.
11. McNeal SI, LeGolvan MP, Chung CS, Ayala A. The dual functions of receptor interacting protein 1 in fas-induced hepatocyte death during sepsis. *Shock* 2011;**35**:499−505.
12. Jouan-Lanhouet S, Arshad MI, Piquet-Pellorce C, Martin-Chouly C, Le Moigne-Muller G, Van Herreweghe F, et al. TRAIL induces necroptosis involving RIPK1/RIPK3-dependent PARP-1 activation. *Cell Death Differ* 2012;**19**:2003−14.
13. Najjar M, Saleh D, Zelic M, Nogusa S, Shah S, Tai A, et al. RIPK1 and RIPK3 kinases promote cell-death-independent inflammation by toll-like receptor 4. *Immunity* 2016;**45**:46−59.
14. Wu Y, Dong G, Sheng C. Targeting necroptosis in anticancer therapy: mechanisms and modulators. *Acta Pharm Sin B* 2020;**10**:1601−18.
15. Zhuang C, Chen F. Small-molecule inhibitors of necroptosis: current status and perspectives. *J Med Chem* 2020;**63**:1490−510.
16. Degterev A, Ofengeim D, Yuan J. Targeting RIPK1 for the treatment of human diseases. *Proc Natl Acad Sci U S A* 2019;**116**:9714−22.
17. Zhu K, Liang W, Ma Z, Xu D, Cao S, Lu X, et al. Necroptosis promotes cell-autonomous activation of proinflammatory cytokine gene expression. *Cell Death Dis* 2018;**9**:500.
18. Degterev A, Hitomi J, Germscheid M, Ch'en IL, Korkina O, Teng X, et al. Identification of RIP1 kinase as a specific cellular target of necrostatins. *Nat Chem Biol* 2008;**4**:313−21.
19. Degterev A, Huang Z, Boyce M, Li Y, Jagtap P, Mizushima N, et al. Chemical inhibitor of nonapoptotic cell death with therapeutic potential for ischemic brain injury. *Nat Chem Biol* 2005;**1**:112−9.
20. Yuan J, Amin P, Ofengeim D. Necroptosis and RIPK1-mediated neuroinflammation in CNS diseases. *Nat Rev Neurosci* 2019;**20**:19−33.
21. Teng X, Degterev A, Jagtap P, Xing X, Choi S, Denu R, et al. Structure–activity relationship study of novel necroptosis inhibitors. *Bioorg Med Chem Lett* 2005;**15**:5039−44.
22. Harris PA, Berger SB, Jeong JU, Nagilla R, Bandyopadhyay D, Campobasso N, et al. Discovery of a first-in-class receptor interacting protein 1 (RIP1) kinase specific clinical candidate (GSK2982772) for the treatment of inflammatory diseases. *J Med Chem* 2017;**60**:1247−61.
23. Harris PA, King BW, Bandyopadhyay D, Berger SB, Campobasso N, Capriotti CA, et al. DNA-encoded library screening identifies benzo [*b*][1,4]oxazepin-4-ones as highly potent and monoselective receptor interacting protein 1 kinase inhibitors. *J Med Chem* 2016;**59**:2163−78.
24. Harris PA, Marinis JM, Lich JD, Berger SB, Chirala A, Cox JA, et al. Identification of a RIP1 kinase inhibitor clinical candidate (gsk3145095) for the treatment of pancreatic cancer. *ACS Med Chem Lett* 2019;**10**:857−62.
25. Berger SB, Harris P, Nagilla R, Kasparcova V, Hoffman S, Swift B, et al. Characterization of GSK'963: a structurally distinct, potent and selective inhibitor of RIP1 kinase. *Cell Death Dis* 2015;**1**:15009.

26. Harris PA, Faucher N, George N, Eidam PM, King BW, White GV, et al. Discovery and lead-optimization of 4,5-dihydropyrazoles as mono-kinase selective, orally bioavailable and efficacious inhibitors of receptor interacting protein 1 (RIP1) kinase. *J Med Chem* 2019;**62**: 5096−110.
27. Rigel Pharmaceuticals. Lilly and Rigel enter strategic collaboration to develop RIPK1 inhibitors for the potential treatment of immunological and neurodegenerative diseases. Available from: https://www.rigel.com/investors/news-events/press-releases/detail/307/lilly-and-rigel-enter-strategic-collaboration-to-develop; Feb 18, 2021.
28. Chen X, Zhuang C, Ren Y, Zhang H, Qin X, Hu L, et al. Identification of the Raf kinase inhibitor TAK-632 and its analogues as potent inhibitors of necroptosis by targeting RIPK1 and RIPK3. *Br J Pharmacol* 2019;**176**:2095−108.
29. Zhang H, Xu L, Qin X, Chen X, Cong H, Hu L, et al. *N*-(7-Cyano-6-(4-fluoro-3-(2-(3-(trifluoromethyl)phenyl)acetamido)phenoxy)benzo [*d*] thiazol-2-yl)cyclopropanecarboxamide (TAK-632) analogues as novel necroptosis inhibitors by targeting receptor-interacting protein kinase 3 (RIPK3): synthesis, structure–activity relationships, and *in vivo* efficacy. *J Med Chem* 2019;**62**:6665−81.
30. Okaniwa M, Hirose M, Arita T, Yabuki M, Nakamura A, Takagi T, et al. Discovery of a selective kinase inhibitor (TAK-632) targeting pan-RAF inhibition: design, synthesis, and biological evaluation of C-7-substituted 1,3-benzothiazole derivatives. *J Med Chem* 2013;**56**:6478−94.
31. Qin X, Hu L, Shi SN, Chen X, Zhuang C, Zhang W, et al. The Bcr-Abl inhibitor GNF-7 inhibits necroptosis and ameliorates acute kidney injury by targeting RIPK1 and RIPK3 kinases. *Biochem Pharmacol* 2020;**177**:113947.
32. Wang Y, Ma H, Huang J, Yao Z, Yu J, Zhang W, et al. Discovery of bardoxolone derivatives as novel orally active necroptosis inhibitors. *Eur J Med Chem* 2021;**212**:113030.
33. Xia C, Yao Z, Xu L, Zhang W, Chen H, Zhuang C. Structure-based bioisosterism design of thio-benzoxazepinones as novel necroptosis inhibitors. *Eur J Med Chem* 2021;**220**:113484.
34. He S, Wang L, Miao L, Wang T, Du F, Zhao L, et al. Receptor interacting protein kinase-3 determines cellular necrotic response to TNF-alpha. *Cell* 2009;**137**:1100−11.
35. Cho YS, Challa S, Moquin D, Genga R, Ray TD, Guildford M, et al. Phosphorylation-driven assembly of the RIP1–RIP3 complex regulates programmed necrosis and virus-induced inflammation. *Cell* 2009;**137**:1112−23.
36. Duprez L, Takahashi N, Van Hauwermeiren F, Vandendriessche B, Goossens V, Vanden Berghe T, et al. RIP kinase-dependent necrosis drives lethal systemic inflammatory response syndrome. *Immunity* 2011;**35**:908−18.
37. Rachmilewitz D, Karmeli F, Takabayashi K, Hayashi T, Leider-Trejo L, Lee J, et al. Immunostimulatory DNA ameliorates experimental and spontaneous murine colitis. *Gastroenterology* 2002;**122**: 1428−41.
38. Ma H, Wu Y, Zhang W, Zhang H, Miao Z, Zhuang C. Radiosensitization of human pancreatic cancer by piperlongumine analogues. *Chin Chem Lett* 2021;**32**:1197−201.